Study of the phase transition sequence of mixed silver tantalate-niobate ($AgTa_{1-x}Nb_xO_3$) by inelastic light scattering

1992 J. Phys.: Condens. Matter 4 2333

(http://iopscience.iop.org/0953-8984/4/9/026)

J. Phys.: Condens. Matter 4 (1992) 2333–2345. Printed in the UK

Study of the phase transition sequence of mixed silver tantalate–niobate ($AgTa_{1-x}Nb_xO_3$) by inelastic light scattering

M Hafid†, G E Kugel†, A Kania‡, K Roleder‡ and M D Fontana†
† Centre Lorrain d'Optique et Electronique du Solide, Université de Metz, Supelec, 2 rue Edouard Belin, 57078 Metz Cédex 3, France
‡ Institute of Physics, Silesian University, 40007 Katowice, Uniwersytecka 4, Poland

Received 18 March 1991, in final form 23 July 1991

Abstract. Light scattering measurements have been performed on single crystals of the solid solution of silver tantalate–niobate in a temperature range extending from 10 K to about 800 K. The experimental results are analysed and discussed by comparison with dielectric and structural data as functions of temperature and relative Nb and Ta concentrations. The specific contributions of each constituent ion to the phase transition sequence and mechanisms are critically discussed.

1. Introduction

The technical importance of the ABO_3 oxidic perovskite compounds in piezoelectricity, photorefractivity (Günter and Huignard 1987), modern optics (Lines and Glass 1977, Voges 1987) as well as superconductivity (Bednorz and Müller 1988) is well known. Their properties have been proved to be strongly dependent on structural and compositional aspects.

The most relevant microscopic parameters influencing modifications in the physical properties are mainly atomic and ionic radius, lattice parameters of the compound, ionicity and covalency of the bonds, local potentials, polarizabilities of the ions and the bonds, nature and concentration of the introduced defects.

In previous papers, the present authors (Kugel *et al* 1984, 1985, 1987a, b, 1988, Fontana *et al* 1984) have investigated the mixed $KTa_{1-x}Nb_xO_3$ system (abbreviated as KTN) using several experimental techniques and as functions of increasing Nb concentration and temperature. The gradual increasing of niobium contents in $KTaO_3$ leads, first, to the appearance of a low-temperature rhombohedral phase, and then to the typical phase transition sequence (cubic, tetragonal, orthorhombic and rhombohedral phases). It has been shown that this is mainly due to two features:

(i) the enhancement of a non-linear polarizability in the O–B bond due to the specific behaviour of the oxygen electronic cloud (Kugel *et al* 1987a, b, 1988, Fontana *et al* 1990);

(ii) the occurrence of a strong relaxational behaviour in the Nb ion dynamics (Fontana *et al* 1988).

0953-8984/92/092333 + 13 $04.50

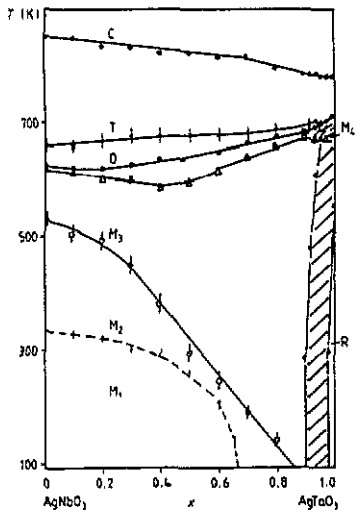

Figure 1. Phase diagram of the $AgTa_{1-x}Nb_xO_3$ solid solution, T, O, R and M describe distortion of the pseudocubic perovskite unit cell of tetragonal, orthorhombic, rhombohedral and monoclinic symmetry. The dashed zones are zones with phase coexistence (Pawelczyk 1987).

In the present paper, we aim to study a new mixed perovskite system $AgTa_{1-x}Nb_xO_3$ hereafter called ATN. Compared to the potassium ion of the KTN system, the silver ion presents quite different microscopic properties, such as for instance smaller ionic radius, higher electronic density and stronger electronic cloud deformability. These characteristics enable strong electronic contributions to delocalized electron density and to ionic and bond polarizabilities, which are known to be of major importance in inductive properties.

The approach of our study is both experimental and theoretical. We performed complete Raman spectroscopy measurements on single crystals of ATN with several Nb concentrations and as a function of temperature; the Raman results are analysed using an adapted light scattering response function yielding the parameters characterizing the dynamics involved in the scattering process. These different results are then discussed critically in order to understand the specific role of each constitutive ion of the system.

2. Phase diagram and dielectric properties of the ATN solid solution

2.1. Phase diagram of the ATN system

The phase diagram of the ATN system as represented on figure 1 (Pawelczyk 1987) exhibits a complex sequence of phase transitions with several antiferrodistorsive transitions at high temperatures. In $AgNbO_3$, the transition temperatures are spread out in a large temperature range and, starting from the high-temperature cubic phase (C), lead to phases with tetragonal (T), orthorhombic (O) and monoclinic (M_1, M_2, M_3) distortions of the pseudoperovskite unit cell. In $AgTaO_3$, the transitions, located between 650 and 770 K, occur between cubic phase (C) and phases with tetragonal (T) and rhombohedral (R) distortions of the pseudocubic unit cell. Coexistence of phases has been detected (see figure 1).

The high-temperature transitions show only a small dependence on Nb concentration; on the contrary, strong modifications in the transition sequence are yielded by the introduction of a small amount of Nb (about 1%) into pure $AgTaO_3$. Furthermore,

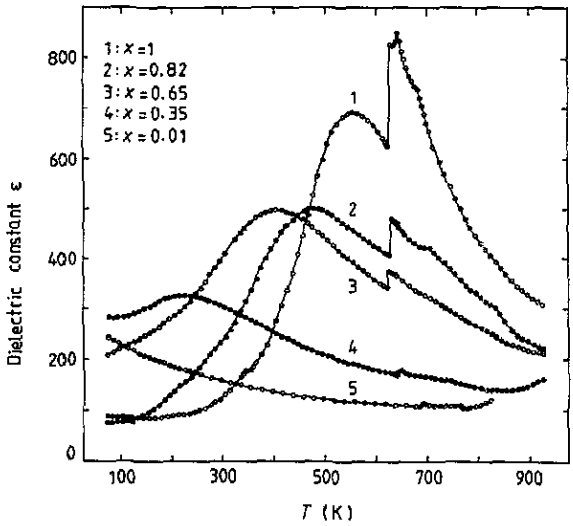

Figure 2. Temperature dependences of the electric permittivity for (1) $AgNbO_3$, (2) $AgTa_{0.18}Nb_{0.82}O_3$, (3) $AgTa_{0.36}Nb_{0.64}O_3$, (4) $AgTa_{0.64}Nb_{0.36}O_3$ and (5) $AgTaO_3$ crystals.

strong changes are observed in the low-temperature phase transitions between the monoclinic phases.

2.2. Dielectric properties of the ATN system

Dielectric measurements (Kania 1983) were performed on ceramics of the ATN system. Similar results obtained for ATN crystals with an electric field of 1 MHz applied with silver electrodes are shown in figure 2. As seen in this figure, the phase transitions are indicated by typical steps and bumps in the dielectric constant–temperature curves. The gradual introduction of Nb concentration yields a strong increasing of the dielectric maximum values, especially due to the enhancement of the large bump, the maximum of which corresponds to the M_2–M_3 phase transition. This bump, which seems to yield the main contribution to the dielectric susceptibility, is shifted towards lower temperature on decreasing the Nb concentration. Since the anomalies at the different T_c values are less pronounced for low-Nb samples, it seems that these transitions are only weakly connected with polarization properties.

3. Dynamic properties of $AgNbO_3$ and $AgTaO_3$

Since the Raman scattering measurements on pure $AgNbO_3$ and $AgTaO_3$ have already been published in earlier papers (Kania *et al* 1986, Kugel *et al* 1987a, b), we summarized here only the main results in order to ensure a global and coherent explanation for the mixed system.

3.1. Raman results on the $AgTaO_3$ crystal

Figure 3 represents three Raman spectra denoted I, II and III and corresponding to high (775 K), room (290 K) and low temperature (10 K). The high-temperature spectrum is

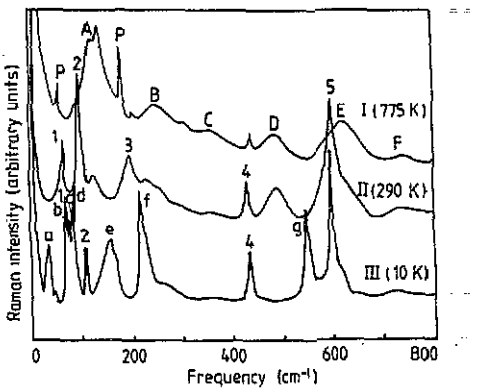

Figure 3. Raman spectra recorded in $AgTaO_3$ crystal at high (775 K), room (290 K) and low temperature (10 K).

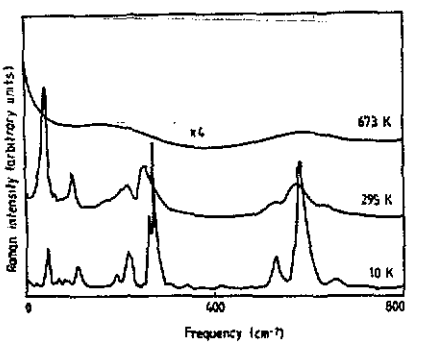

Figure 4. Raman spectra recorded in $AgNbO_3$ crystal at high (673 K), room (295 K) and low temperature (10 K).

recorded in the cubic paraelectric phase and shows several broad bands labelled A, B, C, D, E and F, which have been assigned as second-order scattering lines (Kugel *et al* 1987a, b). The room-temperature spectrum exhibits additional new lines of first order due to the existence of the rhombohedral phase. The peak 1 has been shown to display a soft mode behaviour with increasing temperature to the cubic phase.

In the low-temperature spectrum, new thin lines denoted a, b, c, e, f and g and appearing at 32, 76, 82, 85, 152, 215 and 544 cm^{-1} give evidence of a supplementary structural phase transition that has not been detected by Pawelczyk (1987). This transition has been observed at 170 K on heating and at 120 K on cooling (Kugel *et al* 1987a, b).

3.2. Raman results on the $AgNbO_3$ crystal

In figure 4 are represented the Raman spectra recorded on $AgNbO_3$ at high (673 K), room (295 K) and low temperature (10 K). In accordance with the phase diagram of figure 1, no phase transition occurs below room temperature. Contrary to $AgTaO_3$, the high-temperature spectrum consists of a large quasi-elastic scattering and two broad bands at 200 and 600 cm^{-1}. As reported in figure 5 and as studied in detail by Kania *et al* (1986), the temperature-dependent spectrum of $AgNbO_3$ exhibits, together with and coupled to a low-frequency mode, a particularly high quasi-elastic diffusion. The maximum of this diffusion occurs simultaneously with the structural phase transition M_2–M_3. The low-frequency mode softens with the increase of this central diffusion, persists strongly damped after the M_2–M_3 transition and finally disappears at the O–T transition.

4. Raman results on the mixed $AgTa_{1-x}Nb_xO_3$ system

4.1. Experimental conditions

The Raman measurements were performed on several ATN crystals (Kania 1989) with parallelepipedic shape of about $2 \times 2 \times 1$ mm^3 of slightly brown yellow colour. The

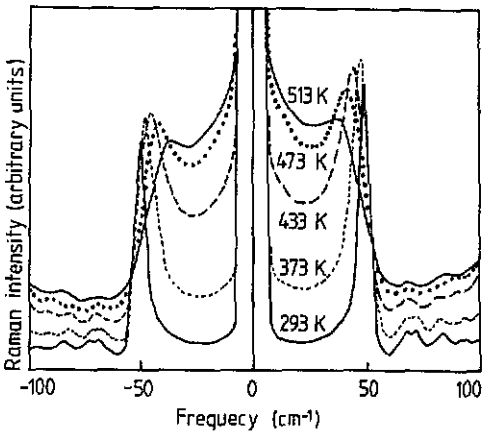

Figure 5. Temperature-dependent Stokes and anti-Stokes low-frequency Raman spectra recorded in $AgNbO_3$.

investigated crystals present niobium molar ratio concentrations of 0.01, 0.02, 0.11, 0.21, 0.35, 0.65 and 0.82.

The experiments have been carried out on a Spex double monochromator model 1401 using a photon counting system and linked with a Datamate microprocessed spectrometer controller and acquisition processor. For high-temperature measurements the samples were mounted in a temperature-controlled furnace allowing temperatures up to 900 K detected with a chromel–alumel thermocouple located near to the sample. For low-temperature measurements, the crystals were cooled down within an Air-Product Displex cryostat driven by an automatic indicator–controller.

4.2. Influence of Nb introduction on the low-temperature Raman spectra

In figure 6 are reported the low-temperature (10 K) Raman spectra recorded in the various ATN crystals. As already observed in $AgNbO_3$ and in $AgTaO_3$ and in accordance with the low symmetry of the crystal, the spectra show a complex structure with several lines located at positions depending strongly on the composition of the mixed system.

For the low-Nb crystals (1% and 2%), the spectra are similar in frequency and relative intensity to those of $AgTaO_3$; the various lines can be assigned comparatively as in section 3.1.

For Nb concentration higher than 2%, an essential modification is observed in the scattered intensities of the lines at 280 and 580 cm^{-1}, which increase gradually with increasing Nb concentration, and corresponds to the main diffusion intensity for highly Nb concentrated samples (see figure 4).

4.3. Influence of Nb introduction on the low-temperature phase transition

In figure 7, the Raman spectra at 10 K and at room temperature are presented for crystals with 1% Nb (ATN1) and 2% Nb (ATN2). A major difference appears: the ATN1 spectrum behaves equivalently to pure $AgTaO_3$. On the contrary, the persistence of several lines (a, c, d) in the room-temperature spectrum of ATN2 indicates a drastic modification in the phase transition sequence induced by 1% additional Nb ions.

In the crystals with higher Nb concentration, the same behaviour occurs:

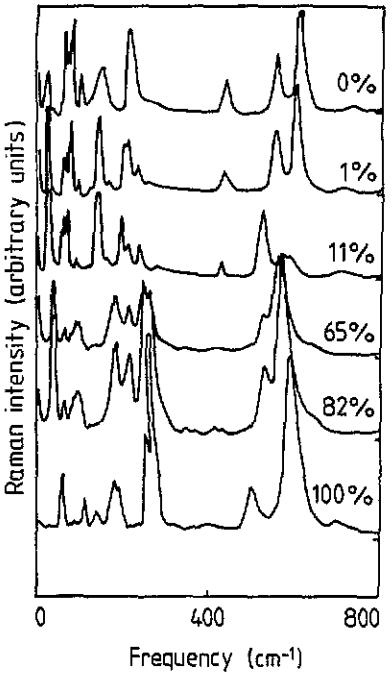

Figure 6. Low-temperature (10 K) Raman spectra recorded in the $AgTa_{1-x}NB_xO_3$ system for various (0%, 1%, 11%, 65%, 82% and 100%) Nb contents.

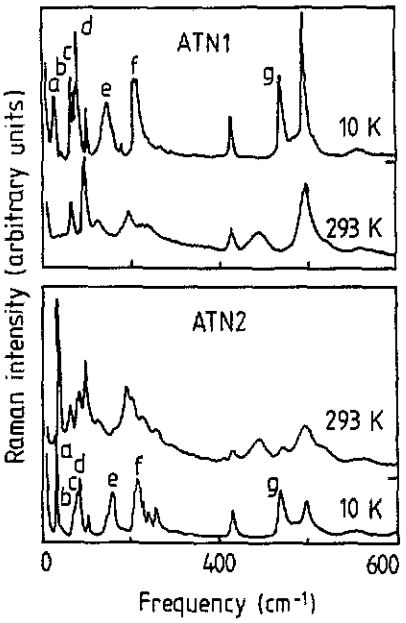

Figure 7. Raman spectra for $AgTa_{0.99}Nb_{0.01}O_3$ (ATN1) and $AgTa_{0.98}Nb_{0.02}O_3$ (ATN2) single crystals at selected temperatures.

(i) the vanishing of the lines b, e, f and g reveals the occurrence of the low-temperature transition (which may be the M_1–M_2 transition);

(ii) the persistence of the other lines (a, c and d) and their disappearance at the transition to the tetragonal phase.

4.4. Investigation of the quasi-elastic diffusion as a function of temperature

In figures 8 and 9 are reported typical examples of the low-frequency Raman spectra measured in samples containing 82% and 21% Nb respectively. As already mentioned in pure $AgNbO_3$, the M_2–M_3 phase transition is accompanied by a maximization in the quasi-elastic diffusion coupled to the low-frequency mode (labelled a), which simultaneously shows a softening. This mode finally vanishes at the O–T transition. In section 5.2, this specific behaviour will be analysed theoretically and the parameters of the coupled excitations involved in the light scattering are determined as functions of temperature and Nb concentration.

4.5. Raman spectra in the vicinity of the high-temperature transitions and in the cubic phase

In figure 10 are reported the Raman spectra of ATN2 above room temperature. The following features are observed:

(i) disappearance of the peak a at 37 cm^{-1} at the O–T phase transition;

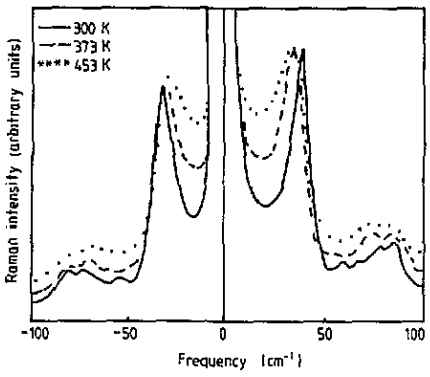

Figure 8. Temperature-dependent low-frequency Raman spectra in $AgTa_{1-x}Nb_xO_3$ with $x = 0.82$.

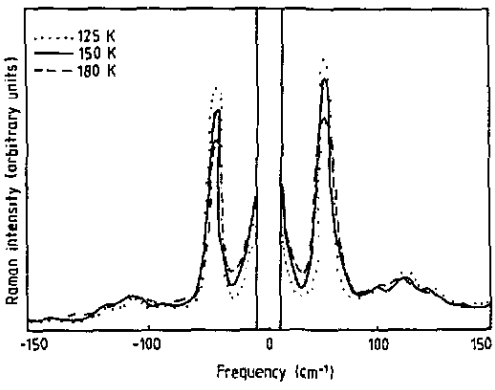

Figure 9. Temperature-dependent low-frequency Raman spectra in $AgTa_{1-x}Nb_xO_3$ with $x = 0.21$.

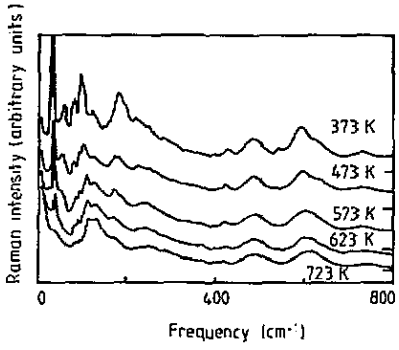

Figure 10. Raman spectra in the high-temperature range for $AgTa_{1-x}Nb_xO_3$ with $x = 0.02$ (ATN2).

(ii) observation as in pure $AgTaO_3$ (line 1 in figure 3) of a soft mode presenting a strong damping inside the T phase;

(iii) occurrence of an intense second-order spectrum.

An equivalent behaviour is detected for the crystals with higher Nb concentrations (11% and 21%). But, with rising Nb content above 21%, these characteristics are gradually attenuated and dominated by the behaviour typical to $AgNbO_3$, i.e.:

(i) occurrence of the quasi-elastic diffusion;

(ii) washing-out of the clear second-order spectra;

(iii) gradual modification of the spectra in a diffusion consisting of a large quasi-elastic part and two large bumps located at 250 and 600 cm^{-1} (figure 4).

It is to be noted that this high-temperature spectrum clearly shows a strong similarity with those observed in $BaTiO_3$ and $KNbO_3$ in their high-temperature phases and in which disordering effects due to off-centring of the Ti and Nb effects have been shown to play a major role (Fontana *et al* 1988, Müller and Berlinger 1986).

5. Analysis and discussion of the Raman results

5.1. Analysis of the low-temperature spectra and connection with ferroelectric properties

The complex low-temperature Raman spectra (figure 6) recorded in the mixed ATN system show a great number of lines of various intensities, which result from mode activations through the successive symmetry breakings due to the structural phase transitions. Owing to the low symmetry and the high complexity of the phases at low temperature, it is impossible to give a detailed line assignment. As usual in perovskite oxides, three main frequency ranges can be distinguished:

(i) a low-frequency part below 200 cm^{-1},
(ii) an intermediate one between 200 and 400 cm^{-1}, and
(iii) a high-frequency range above 400 cm^{-1}.

By comparison with the Raman spectra in $KNbO_3$ and following the notation adopted in this system (Fontana *et al* 1984), the low-frequency bands mainly involve phonons issued from the acoustic and the lowest optic branches activated from Brillouin zone foldings. Inside the b and c ranges, we mentioned, in section 4.2, the strong intensity enhancement of the lines at 280 and 580 cm^{-1} when increasing the Nb concentration. Equivalent strong lines have been detected in other oxygen octahedra compounds containing Nb ions such as $KNbO_3$ (Fontana *et al* 1981, 1985). By comparison with these crystals, the lines at 280 and 580 cm^{-1} can be assigned as vibrations originating from the cubic F_{1u} (TO_1) and F_{1u} (TO_3) modes respectively. In the cubic phase, the TO_1 mode corresponds to the antiphase motion of Nb and the oxygen octahedron. The TO_3 mode consists of a deformation of the oxygen octahedron (with motions of the O located along Oz in opposition to those located along O*x* and O*y*) and small amplitude of the A ions. The Raman cross-sections of both these modes are strongly enhanced by substituting Ta by Nb ions. This indicates that the Nb ions act very sensitively on non-linear susceptibility, leading, in particular, to Raman scattering increasing (Kugel *et al* 1987a, b).

Our Raman results have clearly pointed out that in $AgTaO_3$ and ATN with Nb concentration lower than 2%, a supplementary structural phase transition takes place at a temperature depending on the Nb content x (on heating, 170 K for $x = 0$, about 190 K for $x = 0.01$). For higher Nb content, such a low-temperature transition still exists; but the transition is certainly of different type since several Raman structures persist in the high-temperature phase.

Some small indications of ferroelectricity appearance have been observed in the ATN compounds by pyroelectric measurements (Kania *et al* 1984) at the same temperatures as in our measurements. Nevertheless, since the spontaneous polarization is very small, it is difficult to speak about proper ferroelectricity.

5.2. Analysis of the low-frequency mode and the quasi-elastic diffusion by a coupled phonon-relaxation model and dielectric behaviour

Before giving a theoretical treatment of the low-frequency spectrum, let us summarize the main features describing the corresponding temperature-dependent phenomena observed in the mixed system:

(i) occurrence, in addition to the low-frequency mode, of a particularly anomalous quasi-elastic scattering, which is widely spread out in a large frequency range and in a large temperature region;

(ii) increasing of the intensity of this diffusion, with a maximum at the M_2–M_3 phase transition, then gradual lowering until disappearance;

(iii) increase of its intensity accompanied by a gradual softening of the low-frequency mode;

(iv) persistence of this mode at higher temperatures as a damped low-frequency shoulder disappearing at a higher structural phase transition O–T;

(v) amplitude of the quasi-elastic scattering and its coupling to the low-frequency mode decreasing with lowering Nb content and even unobservable for Nb < 11%; in this case, the low-frequency mode is stable in frequency with increasing temperature.

Complementary with the analysis provided on pure $AgNbO_3$ (Fontana *et al* 1985, Kania *et al* 1986), these data are treated using a suitable lineshape Raman function assuming two dynamic excitations with two different timescales. The first one consists of a resonator and corresponds to the low-frequency mode; the second one to a relaxator giving the broad central component.

For the same reasons as in pure $AgNbO_3$, such as, for instance, the occurrence of excitations in the same frequency range, transfer of scattering intensity between them and correlated behaviour, an accurate fit of the temperature- and Nb concentration-dependent Raman data needs the introduction of coupling between the two excitations. Of course, this interaction parameter is only fully justified for high Nb concentrated samples. Nevertheless, as pointed out later, its consideration in the whole ATN series allows one to study coherently with $AgNbO_3$ the specific (and decreasing) role of the Nb ion on the dynamic and dielectric properties of the system.

The frequency-dependent response function (Fleury 1972, Shapiro *et al* 1973, Riste *et al* 1972) used in our calculations is written as:

$$S(\omega) = \frac{\omega[n(\omega)+1]}{\pi} \frac{\gamma_o + \delta^2\tau/(1+\omega^2\tau^2)}{[\omega_0^2 - \delta^2\tau/(1+\omega^2\tau^2) - \omega^2]^2 + \omega^2[\gamma_0 + \delta^2\tau/(1+\omega^2\tau^2)]^2}$$

where $n(\omega)$ is the thermal Bose–Einstein factor, γ_0 is the normal phonon damping constant, ω_0 is the quasi-harmonic phonon frequency, γ_r is related to the relaxation time (τ) of the relaxator by $\gamma_r = 1/\tau$ and δ^2 is the coupling constant between the two excitations.

The Raman data have been fitted with the previous equation using as adjustable parameters the quantities γ_0, ω_0, δ^2 and $\tau = 1/\gamma_r$; the calculations have been performed in a wide temperature range and, in particular, in order to ensure good starting conditions, for temperatures where the soft-phonon line and the relaxation band can be clearly separated. The fitting parameters γ_r, δ^2, γ_0 and ω_0 obtained in this analysis are plotted as functions of temperature in figures 11, 12 and 13 respectively. The main conclusions that can be deduced from our fits concern successively:

(i) the temperature and Nb dependences of the coupling parameter δ^2;

(ii) the rate of the relaxator γ_r.

For each sample, the coupling constant δ^2 increases on heating up to the M_2–M_3 phase transition. Its magnitude as well as its variation depends strongly on the niobium concentration. Since this quantity reflects the interaction between the two excitations and their intensity transfer, it is obvious that both excitations involve niobium ions motions and that their strong coupling seems to be responsible for the phase transition. The diminution of the Nb concentration weakens this interaction and, consequently,

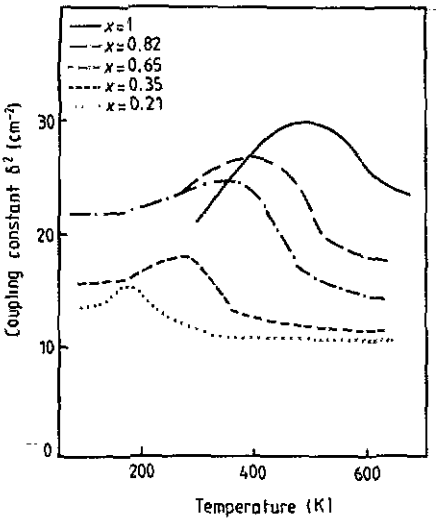

Figure 11. Temperature and Nb concentration dependences of the coupling constant between the relaxation and the soft mode.

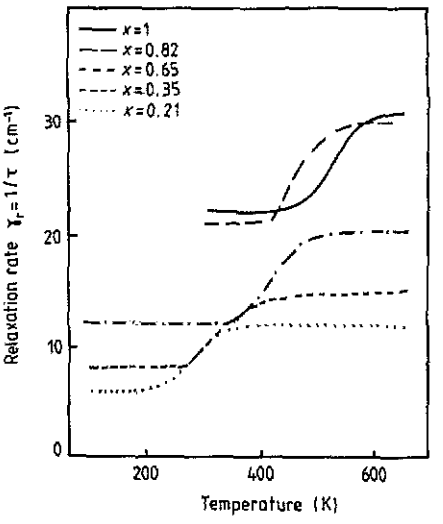

Figure 12. Temperature and Nb concentration dependences of the inverse relaxation time (τ) to the relaxational motion associated to the central diffusion.

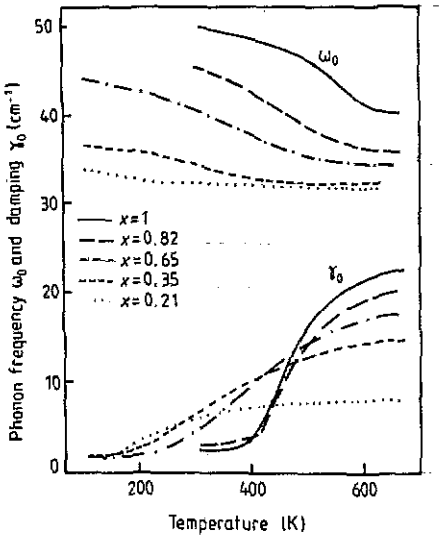

Figure 13. Temperature and Nb concentration dependences of the frequency and the damping of the lowest-phonon mode.

pushes the M_2–M_3 transition down in temperature which obviously presents a pronounced diffuse character. The special temperature behaviour exhibited by δ^2 can be compared with the dielectric temperature function as represented by figure 2. This comparison clearly points out that the origin of the broad bump in ε around M_2–M_3 and its dependence on x is due to the relaxational character of the Nb ion motions and to the coupling between the two excitations. The large values of γ_r, specially for high Nb contents, explains why the central diffusion is observable so clearly by means of Raman scattering. Furthermore, the stabilization of this value in the M_3 phase indicates the

existence of high-frequency relaxation in the Nb lattice, the dynamics of which are the cause of defects and explain the gradual and Nb enhanced smearing out of the first- and second-order Raman structures.

The value of the uncoupled soft-phonon damping γ_0, which is small in the M_2 phase, presents a pronounced rising when approaching the M_2–M_3 transition; its variation also strongly depends on the Nb contents. Similarly, the pseudoharmonic frequency shows, on heating toward the M_2–M_3 transition, a slow and continuous decrease again enhanced by Nb contents.

5.3. Dynamical properties and second-order Raman spectra

As in the case of $AgTaO_3$ (Kugel *et al* 1987a, b), the appearance of the second-order bands A, B, C, D, E and F (figure 3) in the paraelectric phase of the ATN samples with low Nb concentration originates from the same interactions as those acting in other perovskite oxides such as KTN (Nilsen and Skinner 1967, 1968, Kugel *et al* 1985) and $SrTiO_3$ (Migoni *et al* 1976). In these compounds, it has been shown that the strong second-order process is related to an anharmonic fourth-order coupling between the core and the shell of the oxygen ion along the O–B directions. This coupling is described as an anisotropic and non-linear polarizability of the oxygen ion induced by neighbouring ions and is responsible for the mode softening and, in KTN, for the transition to the ferroelectric phase. In ATN, the existence of second-order lines indicates that such a non-linear polarizability is present. Nevertheless, since its magnitude is smaller, the induction of a ferroelectric phase cannot occur. Furthermore, such an eventual ferroelectric transition is preceded by an antiferrodistorsive phase transition, which attenuates the chain-like interaction by distorting the O–B chains.

5.4. Discussion and conclusions

The dynamic behaviour as well as the structural phase transition sequence and mechanism of the KTN and ATN systems show both great similarities and deep differences, which are interpreted by the specific and interconnected role of both A (Ag and K) and B (Nb and Ta) ions. In this conclusion, let us particularly advance the influences of substituting potassium by silver, and tantalum by niobium in both systems.

The silver ion presents a smaller ionic radius (1.26 Å) than K^+ ion (1.33 Å), with more external electrons (Kr $4d^9\,5s^1$) and less electronegativity (1.9 compared to 0.8 in Pauling notation) (Pauling 1960). These properties are revealed to have two main substantial effects.

First, they contribute to an enhancement of the hybridization of the bonds involving the Ag ions and, furthermore, since the electronegativity of Ag is of equivalent magnitude as that of Nb or Ta, to a more homogeneously distributed electronic density along the various bonds. Such an effect favours establishment of directional covalent bonds and occurrence of rotations of the octahedra (Thomann 1987) or, in other words, antiferrodistorsive transitions. Nevertheless, we are aware that such a phenomenological description simply based on electronegativity considerations has its own limitations and gives only a qualitative insight. More elaborate electronic structure calculations should be able to improve this model. The phase transition sequence shows that the described effect is more obvious for compounds with high Nb content: this may be due to the special complex stereochemistry of the Nb ions, which also operates in

other ferroelectric compounds such as the tungsten bronze systems (Lines and Glass 1977).

Secondly, one specific ability of the Ag^+ ion is to be mentioned: this ion is well known to favour quadrupolar electronic deformability in order to take ellipsoidal form (Kleppmann and Bilz 1976, Bilz and Weber 1985). Such deformations are produced at the antiferrodistorsive phase transitions as shown by dynamic calculations pointing out that, at the R and M Brillouin zone points, the critical phonon modes imply ionic motions leading to quadrupolar deformation of the Ag^+ ion electronic cloud. This second aspect may also yield a contribution to the antiferrodistorsive character of the transition.

Concerning the role of the B ions, the relative ratio of the Nb and Ta contents in the mixed systems has been shown to have a great influence on the Raman spectra, the phase diagram and the dielectric behaviour. In Ta-rich compounds, the phase transition at low temperature leads to a phase with small indication of ferroelectricity: it is possible that, as in KTN, the non-linear polarizability of the oxygen ion can develop in this case and may be the leading mechanism for this transition. Nevertheless, this interaction is of significantly smaller amplitude than in KTN as revealed by the smaller amplitude of the second-order Raman spectrum.

In Nb-rich compounds, the relaxational character of the Nb ions plays a dominant role. Our experimental and theoretical investigations show that they are responsible for the M_2–M_3 phase transition and yield drastic contributions to the dielectric behaviour as in other perovskite systems (Fontana *et al* 1988). A more complete understanding of these effects asks for measurements as a function of frequency of the dielectric constants in order to have the dispersive behaviour of these contributions. Nevertheless, since these motions are observable in Raman scattering experiments, they must be operating at rather high frequencies. The increasing Nb contents favouring such a high-frequency contribution to the dielectric susceptibility should equivalently and simultaneously lead to an enhancement of its non-linear part, which is not without interest for technical and device applications for this family of compounds.

References

Bednorz J G and Müller K A 1988 *Rev. Mod. Phys.* **3** 585

Bilz H and Weber W 1985 *Latent Images in Silver Halides* ed A Baldiraschi, D Zaya, E Fosatti and M Cosi (Singapore: World Scientific) p 24

Fleury P A 1972 *Comments Solid State Phys.* **4** 149

Fontana M D, Bouziane E and Kugel G E 1990 *J. Phys.: Condens. Matter* **2** 8681–9

Fontana M D and Kugel G E 1985 *Japan. J. Appl. Phys.* **24** 223

Fontana M D, Kugel G E, Kanina A and Roleder K 1985 *International Meeting in Ferroelectricity, Kobe (Japan)*

Fontana M D, Kugel G E, Metrat G and Carabatos C 1981 *Phys. Status Solidi* b **103** 211

Fontana M D, Metrat G, Servoin J L and Gervais F 1984 *J. Phys. C: Solid State Phys.* **16** 483

Fontana M D, Ridah A, Kugel G E and Carabatos-Nedelec C 1988 *J. Phys. C: Solid State Phys.* **21** 5853

Günter P and Huignard J P 1987 *Photorefractive Materials and their Applications I and II* (Berlin: Springer) 60 and 61

Kania A 1983 *Phase Transitions* **3** 131

—— 1989 *J. Cryst. Growth* **96** 703

Kania A and Roleder K 1984 *Ferroelectrics Lett.* **2** 51

Kania A, Roleder K, Kugel G E and Fontana M D 1986 *J. Phys. C: Solid State Phys.* **19** 9

Kania A, Roleder K and Lukaszewski M 1984 *Ferroelectrics* **52** 265

Kleppmann W G and Bilz H 1976 *Commun. Phys.* **1** 105

Kugel G E, Fontana M D, Hafid M, Roleder K, Kania A and Pawelczyk M 1987a *J. Phys. C: Solid State Phys.* **20** 1217
Kugel G E, Fontana M D and Kress W 1987b *Phys. Rev.* B **35** 813
Kugel G E, Fontana M D, Mesli H and Rytz D 1985 *Japan. J. Appl. Phys.* **24** 226
Kugel G E, Mesli H, Fontana M D and Rytz D 1988 *Phys. Rev.* B **37** 5619
Kugel G E, Vogt H, Kress W and Rytz D 1984 *Phys. Rev.* B **30** 985
Lines M E and Glass A M 1977 *Principles and Applications of Ferroelectrics and Related Materials* (Oxford: Clarendon)
Migoni R, Bilz H and Bäuerle D 1976 *Phys. Rev. Lett.* **37** 1155
Müller K A and Berlinger W 1986 *Phys. Rev.* B **34** 6130
Nilsen W G and Skinner J G 1967 *J. Chem. Phys.* **47** 1413
—— 1968 *J. Chem. Phys.* **48** 2240
Pauling L 1960 *The Nature of the Chemical Bond and the Structure of Molecules and Crystals* (Ithaca, NY: Cornell University Press)
Pawelczyk M 1987 *Phase Transitions* **8** 273
Riste T, Sammelsen E J, Otnes K and Feder J 1971 *Solid State Commun.* **9** 1455
Shapiro J M, Axe J D, Shirane G and Riste T 1973 *Phys. Rev.* B **36** 4332
Thomann H 1987 *Ferroelectrics* **73** 183
Voges E 1987 *Electro-optic and Photorefractive Materials* ed P Günter (Berlin: Springer) 132